

01 Jun 2016

## Integrated Microsphere Whispering Gallery Mode Probe for Highly Sensitive Refractive Index Measurement

Hanzheng Wang

Lei Yuan

Cheol-Woon Kim

*Missouri University of Science and Technology, cheol@mst.edu*

Jie Huang

*Missouri University of Science and Technology, jieh@mst.edu*

*et. al. For a complete list of authors, see [https://scholarsmine.mst.edu/nuclear\\_facwork/468](https://scholarsmine.mst.edu/nuclear_facwork/468)*

Follow this and additional works at: [https://scholarsmine.mst.edu/nuclear\\_facwork](https://scholarsmine.mst.edu/nuclear_facwork)



Part of the [Electrical and Computer Engineering Commons](#), and the [Nuclear Engineering Commons](#)

---

### Recommended Citation

H. Wang et al., "Integrated Microsphere Whispering Gallery Mode Probe for Highly Sensitive Refractive Index Measurement," *Optical Engineering*, vol. 55, no. 6, SPIE, Jun 2016.

The definitive version is available at <https://doi.org/10.1117/1.OE.55.6.067105>

This Article - Journal is brought to you for free and open access by Scholars' Mine. It has been accepted for inclusion in Nuclear Engineering and Radiation Science Faculty Research & Creative Works by an authorized administrator of Scholars' Mine. This work is protected by U. S. Copyright Law. Unauthorized use including reproduction for redistribution requires the permission of the copyright holder. For more information, please contact [scholarsmine@mst.edu](mailto:scholarsmine@mst.edu).

# Integrated microsphere whispering gallery mode probe for highly sensitive refractive index measurement

Hanzheng Wang,<sup>a</sup> Lei Yuan,<sup>a</sup> Cheol-Woon Kim,<sup>b</sup> Jie Huang,<sup>a</sup> Xinwei Lan,<sup>a</sup> and Hai Xiao<sup>a,\*</sup>

<sup>a</sup>Clemson University, Department of Electrical and Computer Engineering, Clemson, South Carolina 29634, United States

<sup>b</sup>MO-SCI Corporation, 4040 HyPoint North, Rolla, Missouri 65401, United States

**Abstract.** We report an integrated whispering gallery mode microresonator-based sensor probe for refractive index sensing. The probe was made by sealing a borosilicate glass microsphere into a thin-wall glass capillary pigtailed with a multimode optical fiber. The intensities of the resonant peaks were found decreasing exponentially (linearly in a log scale) with the increasing refractive index of the medium surrounding the capillary. The sensing capability of the integrated probe was tested using sucrose solutions of different concentrations and the resolution was estimated to be about  $2.5 \times 10^{-5}$  in the index range of 1.3458 to 1.3847. The integrated sensor probe may prove useful in many chemical and biological sensing applications where highly sensitive refractive index monitoring is needed. © 2016 Society of Photo-Optical Instrumentation Engineers (SPIE) [DOI: 10.1117/1.OE.55.6.067105]

Keywords: refractive index sensor; whispering gallery modes; optical resonator; thin wall capillary.

Paper 160328 received Mar. 6, 2016; accepted for publication May 25, 2016; published online Jun. 15, 2016.

## 1 Introduction

Fiber optic refractive index (RI) sensors have many important applications in chemical and biological sensing.<sup>1,2</sup> In most practical applications, a fiber RI sensor is preferred to operate in a single-ended probe configuration, or a reflection-mode operation, for convenient sensor insertion and installation. In addition, it is preferred that the sensor probe has good mechanical strength so that the repeated insertion into the sample will not break the probe. Another important feature that is very much desired is the linear relationship between the RI and the sensor output. Many RI sensors have good sensitivity but a nonlinear response. The calibration of such a nonlinear sensor becomes quite cumbersome when quantitative measurement is required. In addition, the measurement accuracy varies in different RI ranges.

Over the years, many approaches have been explored including (but not limited to) interferometers,<sup>3-5</sup> fiber gratings,<sup>6,7</sup> long period fiber gratings,<sup>8-10</sup> surface plasmonic resonance devices,<sup>11</sup> multimode interference devices,<sup>12</sup> attenuated total internal reflectance sensors,<sup>13,14</sup> extraordinary optical transmission devices,<sup>15</sup> photonic crystal fibers,<sup>16</sup> and whispering gallery mode (WGM) optical microresonators<sup>17</sup> and microlasers.<sup>18</sup> These fiber optic devices have a small size and can be used to measure the RI of a sample with a small volume. In general, fiber optic RI sensors have shown relative measurement resolution somewhere between  $10^{-5}$  and  $10^{-4}$  refractive index units (RIUs), depending on the specific technologies being used. This resolution can satisfy most of the application needs.

In recent years, high-Q WGM optical microresonators have attracted great interests due partially to their broad applications toward highly sensitive detection of chemical and biological quantities.<sup>17-23</sup> Light can be effectively trapped inside these small, low-loss, and rotationally symmetric optical resonators. As a result, the light-environment

interaction is accumulated to achieve high detection sensitivity as the light circulates many times around the circumference of the resonator. The effective index of the WGM is a function of the RI of the medium surrounding the microresonator. As such, a microresonator can be used for RI sensing by monitoring its resonance spectrum. This mechanism has been widely used for label-free biological sensing.

However, the highly sensitive microresonators are not easy to use in practical applications. One of the reasons is the necessity of using a thin fiber taper with a diameter of about 1 to 2  $\mu\text{m}$  to couple the light into and out of the resonator. The thin taper is extremely fragile and the coupling requires complicated adjustments. Due to the same reason, most WGM resonators work in transmission mode, making them less convenient in field applications.

Recently, we proposed a fiber pigtailed thin wall capillary coupler for the excitation of microsphere optical microresonator.<sup>24</sup> Comparing with other coupling methods (e.g., prisms and fiber tapers), the alignment-free well-supported coupling structure allows the WGM resonator to operate in a convenient reflection mode. The coupler-resonator integrated device has shown a great potential for various sensing applications. In this study, we report our studies on using such an integrated WGM resonator probe for highly sensitive RI measurement.

## 2 Sensor Structure, Fabrication, and Sensing Mechanism

Figure 1 shows the structure of the integrated WGM resonator probe and the method of interrogation. The coupler was made by fusion splicing a capillary tube (Polymicro Technologies, LLC, ID/OD 75/150  $\mu\text{m}$ ) to a multimode fiber (Corning, Inc. 62.5/125  $\mu\text{m}$ ). At the joint point, a cone shape was formed. A borosilicate glass microsphere with low coefficient of thermal expansion ( $\sim 3 \times 10^{-6} \text{ K}^{-1}$  at 20°C) was inserted into the capillary till in contact with

\*Address all correspondence to: Hai Xiao, E-mail: [haix@clemson.edu](mailto:haix@clemson.edu)

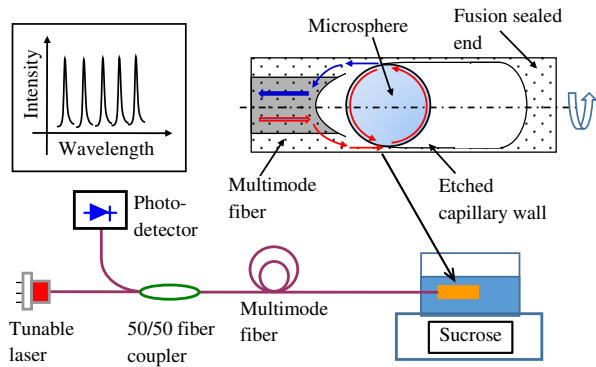


**Fig. 1** Schematic of thin wall capillary coupled borosilicate glass microsphere resonator for RIU sensing.

the capillary wall at the cone portion. The far end of the capillary was then sealed by arc and the entire structure was chemically etched using hydrofluoric acid (Acros Organics, 20%) to reduce the wall thickness down to about  $2 \mu\text{m}$ . The detailed fabrication process and parameters can be found in our previous publication.<sup>24</sup>

To interrogate the integrated microresonator sensor, the light from a tunable laser (Agilent, HP-8168F) was coupled into the sensor through a 50/50 fiber coupler. The light propagating in the multimode fiber entered the capillary thin wall at the cone-shaped joint. The WGMs of the microsphere were excited by the evanescent waves of the light propagating along the capillary thin wall.<sup>24</sup> At the opposite side, the light was coupled out from the microsphere and propagated backwards through the multimode fiber coupler to reach the photodetector (Agilent 8163A). As the tunable laser scanned through its available spectrum range, the resonance spectrum was acquired. As mentioned early, the integrated probe is alignment free and operates in a convenient reflection-mode, which is preferred in many sensing applications.

### 3 Experiments

The integrated probe was immersed in a sucrose solution under room temperature to study its response to surrounding RI changes. The RI of the solution was changed by increasing the sucrose concentrations. The sucrose concentrations of the solution were adjusted to 1.00, 5.00, 8.00, 10.00, 12.00, 14.00, 16.00, 18.00, 20.00, 22.00, 26.00, 28.00, 30.00, and 32.00 in weight percentage, which gave the RIs of the liquid to be 1.3344, 1.3403, 1.3458, 1.3479, 1.3510, 1.3541, 1.3573, 1.3606, 1.3639, 1.3672, 1.3706, 1.3740, 1.3775, 1.3811, and 1.3847, respectively.<sup>25</sup>

Figure 2 shows the resonance spectrum of an integrated WGM probe immersed in deionized (DI) water. The borosilicate glass microsphere inside the probe has a diameter of  $69 \mu\text{m}$ . The spectrum shows a clear periodic resonance pattern. The  $Q$ -factor was calculated to be  $2.55 \times 10^4$  at the resonance wavelength of  $1533.06 \text{ nm}$  where the related full width at half maximum (FWHM) was  $0.06 \text{ nm}$  and the free spectrum range was  $7.69 \text{ nm}$ .

### 4 Results and Discussions

The mode order numbers are also provided in Fig. 2. Compared to fused silica glass microspheres excited by a fiber taper, the  $Q$ -factor of the integrated resonator probe

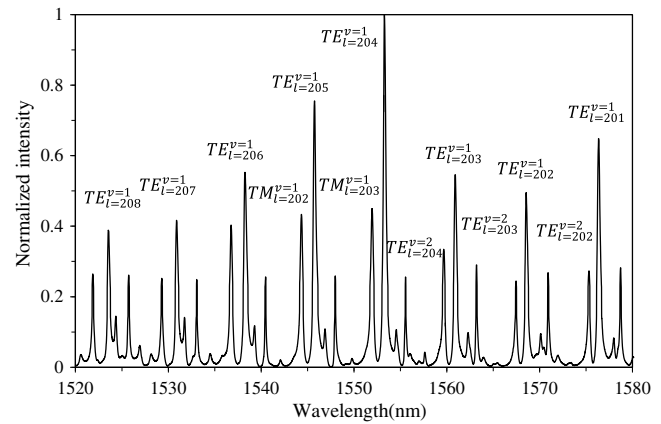


**Fig. 2** Reflection resonance spectrum of the thin wall capillary coupled borosilicate glass microsphere with a diameter of  $69 \mu\text{m}$ .

was significantly lower. The low  $Q$ -factor can be attributed to following possible reasons. From the coupling perspective, the glass sphere was in contact with the inner surface of the capillary. Compared to a fiber taper coupling approach, the capillary gap-free coupling with long sphere-waveguide contact interaction may not support critical coupling. Thus, the higher contact loss could lower the  $Q$ .<sup>24</sup> From the material aspect, the borosilicate glass microsphere had a higher optical loss comparing to the fused silica microsphere. The microsphere surface roughness and unevenness might also contribute to a higher scattering loss and lower  $Q$ .

The evanescent field of the thin capillary waveguide is redistributed when the RI of the surrounding medium changes. As a result, the light coupling between the capillary wall and the microsphere is influenced by the RI of the surrounding medium.

Figure 3 shows the full resonance spectra when the RI changed from 1.3344 to 1.3847 by increasing the sucrose concentration from 1.00 to 32.00 in weight percentage. During the test, the sucrose solution was under constant stirring to ensure a uniform concentration. The resonance spectrum did not have observable changes even when the solution was under constant stirring, indicating the good mechanical stability of the integrated WGM probe.

As shown in Fig. 3, the intensities of the resonance peaks decreased significantly when the RI of the surrounding

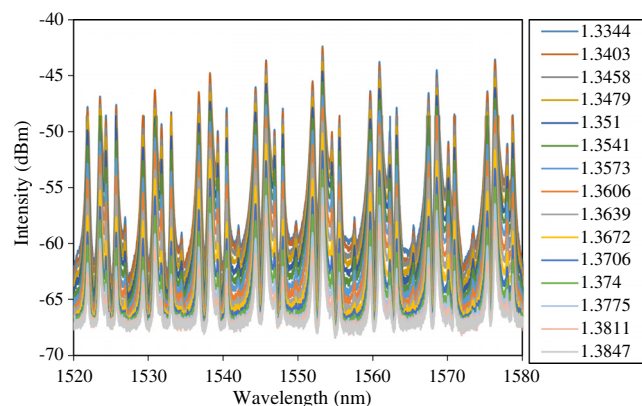


**Fig. 3** Resonance spectra of the integrated probe at different refractive indices by varying the sucrose concentrations.

medium increased. The resonance spectral positions did not have observable changes. The results indicated that the light coupling between the capillary wall and the microsphere was influenced dramatically.

To understand the influence of RI on the light coupling between the microsphere and capillary wall, the resonance peak intensities as a function of the liquid RIs are plotted in Fig. 4. Three different WGMs modes in the wavelength range of 1550 to 1560 nm were selected, including TE ( $v = 1, l = 204$ ), TM ( $v = 1, l = 203$ ), and TE ( $v = 2, l = 204$ ) as shown in the inset of Fig. 4 (highlighted with dash circles and numerical labels).

As shown in Fig. 4, in the range of RI variations, the overall peak intensities decreased monotonically. Except for the first two RI values, the relationship between the RI and peak intensities followed a linear curve in a log scale or exponential in the linear scale. The linear regressions of the three lines (excluding the first two RI values) resulted in slopes of  $-386$ ,  $-413$ , and  $-436$  dBs per unit RI for the peak 1, 2, 3 lines, respectively. The coefficients of determination (or the  $R$ -squared values) of the curve fittings were 0.993, 0.995, and 0.996 for the peak 1, 2, 3 lines, respectively, indicating good linear relations (in a log scale) of the data points.

The general trends of the exponential RI–intensity relation can be qualitatively explained by the asymmetric waveguide model depicted in Fig. 5, where, for simplicity, a slab waveguide ( $n_G$ ) is used to represent the glass capillary wall. The two sides of the slab waveguide are air ( $n_A = 1$ ) and liquid ( $n_L$ ), respectively. The effective RI ( $n_{\text{eff}}$ ) of the guided waves propagating inside the slab waveguide need to satisfy the following total internal reflection condition:

$$n_{\text{eff}} \geq n_L \geq n_A. \quad (1)$$

The penetration depth ( $d$ ) of the evanescent wave on the air side is given as

$$d = \frac{\lambda}{4\pi} (n_{\text{eff}}^2 - n_A^2)^{-1/2}, \quad (2)$$

where  $\lambda$  is the wavelength in vacuum.

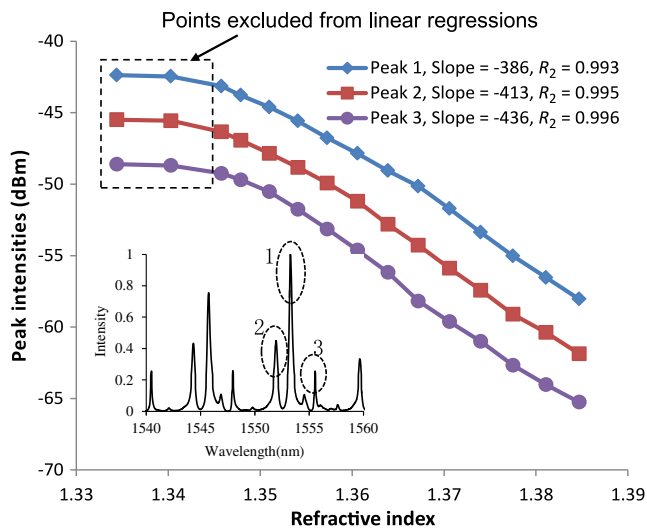


**Fig. 4** Resonance peak intensities as functions of the RIs of the surrounding medium. The slope and  $R$ -squared values are based on the linear regressions of the curves excluding the first two points of each line. Inset: resonance spectrum showing the three peaks analyzed.

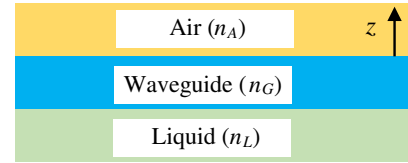


**Fig. 5** Illustration of the asymmetric waveguide model for qualitative understanding of the RI–intensity relation.

When the liquid RI ( $n_L$ ) increases, the effective index of the guide wave ( $n_{\text{eff}}$ ) needs to increase correspondingly to satisfy Eq. (1). Based on Eq. (2), the increased  $n_{\text{eff}}$  will result in a reduced penetration depth. The evanescent field intensity  $I_e(z)$  decays exponentially with the perpendicular distance  $z$  from the interface

$$I_e(z) = I_{e0} \exp\left(-\frac{z}{d}\right), \quad (3)$$

where  $I_{e0}$  is the evanescent field intensity at  $z = 0$ . Equation (3) indicates that the evanescent field intensity drops exponentially as the penetration depth decreases.

The resonance peak intensity of the integrated resonator is determined by the total quality factor ( $Q_T$ ) of the system, which includes the contributions of both the internal quality factor ( $Q_I$ ) and the external (or coupling) quality factor ( $Q_E$ ), given as

$$\frac{1}{Q_T} = \frac{1}{Q_I} + \frac{1}{Q_E}. \quad (4)$$

$Q_E$  is determined by the coefficient of light coupling between the capillary wall and the microsphere, which is proportional to the integral of the evanescent field over their overlapping area. In our case,  $Q_E$  decreases exponentially with the increasing RI of the surrounding medium (i.e., the liquid).

The last procedure in sensor fabrication was to etch the capillary in an HF solution (whose RI was about the same as that of the DI water) while the resonance spectrum was observed in real time.<sup>23</sup> The etching was stopped when the resonance peaks reached their maximum intensities and the system was at the under coupling condition ( $Q_E > Q_I$ ). As a result, the change in  $Q_E$  was less influential on  $Q_T$  because  $Q_I$ 's contribution is still substantial. When  $Q_E$  continue decreases, the peak intensities dropped exponentially with the increasing liquid RIs at the lower portions of the curves in Fig. 4. It should be noted that  $Q_E$  may have a chance to decrease until  $Q_E = Q_I$ , then the critical coupling condition happens. However, the peak intensities of the spectra may not be observed due to the low signal-to-noise ratio and detection limit of the power meter. Overall, the above description only provides a qualitative explanation of the exponential RI–intensity relation. More precise understanding can be obtained by modeling and simulations, which are beyond the scope of this study.

The exponential (or linear in a log scale) RI–intensity relation is particularly useful for RI sensing because it makes the sensor calibration and data interpretation easy. Most optical power meters can easily achieve a measurement resolution of 0.01 dB. Based on the slopes shown in Fig. 4, we estimated that the RI sensing resolution of the sensor was about  $2.5 \times 10^{-5}$  RIU. This resolution satisfies the needs in

most applications. Another advantage of the reported sensor is its sealed and integrated structure. As shown in Fig. 3, the mechanical vibrations resulted from liquid stirring did not affect the reading at all. The reflection-based operation makes the probe easy to use.

## 5 Conclusions

In summary, an integrated WGM microresonator-based probe was developed for RI sensing. The probe was made by sealing a borosilicate glass microsphere into a thin-wall glass capillary pigtailed with a multimode optical fiber. The capillary wall was etched in an HF solution until the system reached the critical coupling condition where the resonance peaks had maximum intensities. When used for RI sensing, the increasing RI of the surrounding medium reduced the penetration depth of the evanescent field of the capillary wall waveguide. Consequently, the external (or coupling)  $Q$  decreased and the intensities of the resonance peaks dropped. When the WGM probe was off the critical coupling condition, the peak intensities were found decreasing exponentially (linear in a log scale) with the increasing RI. This linear in a log scale relation makes it easy to calibrate and interpret the sensor. The measurement resolution was estimated to be about  $2.5 \times 10^{-5}$  RIU in the index range of 1.3458 to 1.3847, with the assumption of 0.01 dB resolution in optical power measurement. Of course, the RI measurement range can be adjusted during the sensor fabrication process. The integrated WGM probe was structurally stable, easy to operate, and useful in chemical and biomedical sensing.

## Acknowledgments

This material was based upon work supported by NIH under contract R21GM104696.

## References

1. X. Fan et al., "Sensitive optical biosensors for unlabeled targets: a review," *Anal. Chim. Acta* **620**(1), 8–26 (2008)
2. X.-D. Wang et al., "Fiber-optic chemical sensors and biosensors," *Anal. Chem.* **85**(2), 487–508 (2013).
3. R. Jha et al., "Ultraprecise reflection photonic crystal fiber modal interferometer for accurate refractive index sensing," *Appl. Phys. Lett.* **93**(19), 191106 (2008).
4. Z. Tian et al., "Refractive index sensor based on an abrupt taper Michelson interferometer in a single-mode fiber," *Opt. Lett.* **33**(10), 1105–1107 (2008).
5. T. Zhaobing et al., "Refractive index sensing with mach&-zehnder interferometer based on concatenating two single-mode fiber tapers," *IEEE Photonics Technol. Lett.* **20**(8), 626–628 (2008).
6. A. Iadicicco et al., "Thinned fiber Bragg gratings as high sensitivity refractive index sensor," *IEEE Photonics Technol. Lett.* **16**(4), 1149–1151 (2004).
7. W. Liang et al., "Highly sensitive fiber Bragg grating refractive index sensors," *Appl. Phys. Lett.* **86**(15), 151122 (2005).
8. V. Bhatia et al., "Applications of long-period gratings to single and multi-parameter sensing," *Opt. Express* **4**(11), 457–466 (1999).
9. H. J. Patrick et al., "Analysis of the response of long period fiber gratings to external index of refraction," *J. Lightwave Technol.* **16**(9), 1606–1612 (1998).
10. V. Bhatia et al., "Optical fiber long-period grating sensors," *Opt. Lett.* **21**(9), 692–694 (1996).
11. X.-B. Zhang et al., "An optical fiber chemical sensor for mercury ions based on a porphyrin dimer," *Anal. Chem.* **74**(4), 821–825 (2002).
12. L. B. Soldano et al., "Optical multi-mode interference devices based on self-imaging: principles and applications," *J. Lightwave Technol.* **13**(4), 615–627 (1995).
13. P. Polykin et al., "Evanescent field-based optical fiber sensing device for measuring the refractive index of liquids in microfluidic channels," *Opt. Lett.* **30**(11), 1273–1275 (2005).
14. J. Villatoro et al., "Low-cost optical fiber refractive-index sensor based on core diameter mismatch," *J. Lightwave Technol.* **24**(3), 1409–1413 (2006).
15. X. Lan et al., "Reflection based extraordinary optical transmission fiber optic probe for refractive index sensing," *Sens. Actuators B* **193**, 95–99 (2014).
16. D. K. C. Wu et al., "Ultrasensitive photonic crystal fiber refractive index sensor," *Opt. Lett.* **34**(3), 322–324 (2009).
17. V. S. Ilchenko et al., "Optical resonators with whispering-gallery modes-part II: applications," *IEEE J. Select. Topics Quantum Electron.* **12**(1), 15–32 (2006).
18. V. D. Ta et al., "Whispering gallery mode microlasers and refractive index sensing based on single polymer fiber," *Laser Photonics Rev.* **7**(1), 133–139 (2013)
19. M. Cai et al., "Observation of critical coupling in a fiber taper to a silica-microsphere whispering-gallery mode system," *Phys. Rev. Lett.* **85**(1), 74–77 (2000).
20. C. Y. Chao et al., "Biochemical sensors based on polymer microrings with sharp asymmetrical resonance," *Appl. Phys. Lett.* **83**(8), 1527–1529 (2003).
21. N. M. Hanumegowda et al., "Aqueous mercuric ion detection with microsphere optical ring resonator sensors," *Sens. Actuators, B* **120**(1), 207–212 (2006).
22. H. Wang et al., "Computational modeling and experimental study on optical microresonators using optimal spherical structure for chemical sensing," *Adv. Chem. Eng. Res.* **2**(3), 45–50 (2013).
23. H. Wang et al., "Optical microresonator based on hollow sphere with porous wall for chemical sensing," *Opt. Lett.* **37**(1), 94–96 (2012).
24. H. Wang et al., "Fiber pigtailed thin wall capillary coupler for excitation of microsphere WGM resonator," *Opt. Express* **21**(13), 15834–15839 (2013).
25. D.R. Lide et al., *CRC Handbook of Chemistry and Physics: A Ready-Reference Book of Chemical and Physical Data*, CRC, Boca Raton Fla, (2009).

**Hanzheng Wang** received his PhD in the Electrical Engineering Department at Clemson University in August 2014. He is now an imaging and measurement system engineer at Corning, Inc. His research interest mainly focuses on image processing, machine vision, fiber optics, optical sensors, and optical microresonators for applications in chemical and biomedical sensing. He was awarded Newport Spectra-Physics Research Excellence Awards in 2012 and the SPIE Education and Travel Scholarships in 2014. He is a member of OSA, ISA, and SPIE.

**Lei Yuan** received his PhD in mechanical engineering at Beijing Institute of Technology in June 2014. He is currently pursuing another PhD in electrical engineering at Clemson University. His research interest mainly focuses on ultrafast laser micromachining of novel micro/nano photonic materials, structures, devices and sensors for harsh environment sensing applications. He is an invited member of Phi Kappa Phi Honor Society, and a member of SPIE, OSA, IEEE and LIA.

**Cheol-Woon Kim** is a senior R&D engineer at MO-SCI Corporation. He has expertise in glass/ceramic science and technology such as new glass composition formulation, glass chemistry, structure, optical, mechanical and thermal properties, coating, and processing.

**Jie Huang** received his PhD in electrical engineering at Clemson University in July 2015. His research interest mainly focuses on the development of photonics and microwave sensors and instrumentations for applications in energy, intelligent infrastructure, and biomedical sensing. He was a recipient of the IEEE Instrumentation and Measurement Society Graduate Fellowship Award from 2012 to 2013. He is a member of Omicron Delta Kappa National Leadership Honor Society, and a student member of OSA, SPIE, and IEEE.

**Xinwei Lan** received his PhD in electrical engineering at Missouri University of Science and Technology in 2013. He was a research associate at Clemson University from 2013 to 2014 and he is currently a scientist at Halliburton. His research efforts have been dedicated to developing optical and microwave sensors for harsh environment sensing, chemical/biological sensing, and structure health monitoring. He is a member of SPIE, OSA, IEEE, and ACS.

**Hai Xiao** is the Samuel Lewis Bell Distinguished Professor of Electrical and Computer Engineering and jointly affiliated with COMSET at Clemson University. His research interests mainly focus on photonic and microwave sensors and instrumentation for applications in energy, intelligent infrastructure, clean environment, biomedical sensing/imaging, and national security.